PNAS RESEARCH ARTICLE | NEUROSCIENCE OPEN ACCESS

Endothelial deletion of EPH receptor A4 alters single-cell profile and Tie2/Akap12 signaling to preserve blood–brain barrier integrity

Alison Cash[a,1], Caroline de Jager[b,1], Thomas Brickler[a], Eman Soliman[a], Liliana Ladner[c], Alexandra M. Kaloss[a], Yumeng Zhu[d], Kevin J. Pridham[a], Jatia Mills[a], Jing Ju[a], Erwin Kristobal Gudenschwager Basso[a], Michael Chen[a], Zachary Johnson[e,f], Yianni Sotiropoulos[g], Xia Wang[a], Hehuang Xie[a,e,f,h], John B. Matson[d], Eric A. Marvin[c], and Michelle H. Theus[a,g,2]

Edited by Stefan Liebner, Goethe-Universitat Frankfurt am Main, Frankfurt/Main, Germany; received March 16, 2022; accepted September 6, 2023 by Editorial Board Member Jeremy Nathans

Neurobiological consequences of traumatic brain injury (TBI) result from a complex interplay of secondary injury responses and sequela that mediates chronic disability. Endothelial cells are important regulators of the cerebrovascular response to TBI. Our work demonstrates that genetic deletion of endothelial cell (EC)-specific EPH receptor A4 (EphA4) using conditional *EphA4*$^{f/f}$*/Tie2-Cre* and *EphA4*$^{f/f}$*/VE-Cadherin-CreERT2* knockout (KO) mice promotes blood–brain barrier (BBB) integrity and tissue protection, which correlates with improved motor function and cerebral blood flow recovery following controlled cortical impact (CCI) injury. scRNAseq of capillary-derived KO ECs showed increased differential gene expression of BBB-related junctional and actin cytoskeletal regulators, namely, A-kinase anchor protein 12, *Akap12*, whose presence at Tie2 clustering domains is enhanced in KO microvessels. Transcript and protein analysis of CCI-injured whole cortical tissue or cortical-derived ECs suggests that EphA4 limits the expression of Cldn5, Akt, and Akap12 and promotes Ang2. Blocking Tie2 using sTie2-Fc attenuated protection and reversed Akap12 mRNA and protein levels cortical-derived ECs. Direct stimulation of Tie2 using Vasculotide, angiopoietin-1 memetic peptide, phenocopied the neuroprotection. Finally, we report a noteworthy rise in soluble Ang2 in the sera of individuals with acute TBI, highlighting its promising role as a vascular biomarker for early detection of BBB disruption. These findings describe a contribution of the axon guidance molecule, EphA4, in mediating TBI microvascular dysfunction through negative regulation of Tie2/Akap12 signaling.

brain injury | junction protein | neuroprotection

Significance

The blood–brain barrier (BBB) regulates homeostasis in the brain, and the extent of BBB disruption can dictate neurological outcomes following tissue perturbation. Our work has uncovered a role for EphA4/Tie2/Akap12 signaling in BBB dysfunction and highlights Ang2 as a potential human biomarker for TBI. Overall, these findings provide new mechanistic insights into the pathophysiology of TBI and mediators of blood-brain barrier regulation.

Traumatic brain injury (TBI) is accompanied by a myriad of secondary injury responses that include disruption to the blood–brain barrier (BBB) (1). BBB dysfunction and subsequent edema and inflammation are negative prognostic indicators of the TBI outcome (2). Endothelial cells (ECs) that line blood vessels are connected adjacently by tight junction proteins such as claudins, occludens, and zona occludens (ZO) (2), which control permeability and restrict access to certain large molecules such as the serum protein, albumin, as well as immune cells from entering the brain (3). Disruption of this mechanism allows increased paracellular transport and dysfunctional transcytosis (4). Tight junctional protein expression, which maintains an intact BBB, can be regulated by matrix metalloproteinases (MMPs) and other signaling events, such as endothelial-specific changes involving Tie2/Angiopoietin (5–10). Recent studies suggest that the endothelial expression of ephrin receptor type A4 is a novel regulator of Tie2 in pial collateral vessel remodeling (11); however, its role in regulating tissue damage, BBB dysfunction, and histopathology in models of brain injury remains unexplored.

Eph (erythropoietin-producing human hepatocellular) receptors are essential for axon growth and guidance in the embryonic and early postnatal stages of brain development (12). Bidirectional signaling plays a significant role in regulating Eph/ephrin biology (13). Being the most prominent family of receptor tyrosine kinases, they are subdivided into classes A and B, expressed throughout the body (14, 15). Class A receptors have been implicated in the brain injury response, including regulation of the BBB. EphA6 was shown to be up-regulated following TBI and correlated with a decrease in neurite density and motor function (16), while ephrinB2/EphB4 signaling regulates arterio-venous specification (17). EphA4 loss of function in the bone marrow immune compartment attenuates neuroinflammation and mediates neuroprotection following TBI (18), while activation of EphA2 following ischemic stroke increased BBB permeability and exacerbated injury outcome (19). Therefore, Eph receptors represent a

Author affiliations: [a]Department of Biomedical Sciences and Pathobiology, Virginia Tech, Blacksburg, VA 24061; [b]Translational Biology Medicine and Health Graduate Program, Virginia Tech, Blacksburg, VA 24061; [c]Virginia Tech Carilion School of Medicine, Virginia Tech, Roanoke, VA 24016; [d]Department of Chemistry, Virginia Tech, Blacksburg, VA 24061; [e]Genetics, Bioinformatics and Computational Biology Program, Virginia Tech, Blacksburg, VA 24061; [f]Epigenomics and Computational Biology Lab, Fralin Life Sciences Institute, Virginia Tech, Blacksburg, VA 24061; [g]Summer Veterinary Student Research Program, Virginia-Maryland College of Veterinary Medicine, Virginia Tech, Blacksburg, VA 24061; and [h]Center for Engineered Health, Virginia Tech, Blacksburg, VA 24061

Author contributions: A.C., C.d.J., T.B., L.L., A.M.K., K.J.P., and M.H.T. designed research; A.C., C.d.J., T.B., E.S., L.L., A.M.K., K.J.P., J.J., E.K.G.B., M.C., X.W., E.A.M., and M.H.T. performed research; Y.Z. and J.B.M. contributed new reagents/analytic tools; A.C., C.d.J., T.B., E.S., L.L., A.M.K., K.J.P., J.M., J.J., M.C., Z.J., Y.S., H.X., and M.H.T. analyzed data; and A.C., L.L., H.X., J.M., and M.H.T. wrote the paper.

The authors declare no competing interest.

This article is a PNAS Direct Submission. S.L. is a guest editor invited by the Editorial Board.

[1]A.C. and C.d.J. contributed equally to this work.

[2]To whom correspondence may be addressed. Email: mtheus@vt.edu.

This article contains supporting information online at https://www.pnas.org/lookup/suppl/doi:10.1073/pnas.2204700120/-/DCSupplemental.

Published October 5, 2023.

mechanistic target in the secondary injury response following brain injury.

The current study sought to uncover the cell-autonomous role of EphA4 in regulating functional deficits and endothelial-derived BBB dysfunction in a murine model of TBI using several conditional knockout approaches and single-cell transcriptomic analysis of capillary-derived ECs. Targeted stimulation and inhibition of the Tie2 receptor were further utilized to provide mechanistic insight into the influence of EphA4 on distinct endothelial cell changes controlling BBB function in the injured brain.

Results

EphA4 Expression and Cortical Tissue Damage Following Endothelial- vs. Peripheral Immune–Derived Deletion in CCI Injury. Acute changes in EphA4 expression were evaluated using immunohistochemistry at 1 day post-CCI injury (dpi) in adult male mice. We observed an increase in the expression of EphA4 in the ipsilateral cortex on Cd31-positive microvessels and associated cells (Fig. 1*B*) compared to the contralateral cortex (Fig. 1*A*). Previously, we identified EphA4 expression on Cx3cr1-expressing cells in the damaged cortex following CCI injury (18) and now confirm expression resides on peripheral-derived immune cells using GFP chimeric mice (Fig. 1 *C*, *D*, and *F*). To determine cell-specific function in mediating neural tissue damage, we adopted a chimeric approach using (WT) *EphA4*$^{f/f}$ or (KO) *EphA4*$^{f/f}$*/Tie2-Cre* recipient mice receiving either *EphA4*$^{+/+}$*/Tie2-Cre/Rosa26*^{mTmG} (WT^{WTBMCs}; KO^{WTBMCs}) or *EphA4*$^{f/f}$*/Tie2-Cre/Rosa26*^{mTmG} (WT$^{KO\ BMCs}$; KO$^{KO\ BMCs}$) bone marrow cell (BMC) transfer (Fig. 1*G*). Tie2 is a tyrosine kinase receptor expressed primarily on vascular endothelial cells (7), a subset of monocytes (20), and in the hematopoietic compartment during development (21). We previously confirmed that *EphA4*$^{f/f}$*/Tie2-Cre* mice show gene deletion in endothelial cells and bone marrow–derived immune cells (11, 18, 22). Here, we find that KO$^{KO\ BMC}$ mice showed reduced lesion volume compared to WT$^{WT\ BMC}$ mice, which was partly attenuated when EphA4 was removed from either the BMC or endothelial compartments (WT$^{KO\ BMC}$ vs. KO$^{WT\ BMC}$, respectively) at 1dpi cortical impact. These data suggest that EphA4 mediates tissue damage by regulating endothelial or immune cell–specific functions.

Loss of EphA4 on Tie2-Expressing Cells Limits Tissue Damage, Prevents BBB Disruption, and Improves Functional Recovery. Next, we subjected *EphA4*$^{f/f}$(WT) and *EphA4*$^{f/f}$*/Tie2-Cre* (KO) mice to controlled cortical impact (CCI) injury and evaluated longitudinal histological and functional changes. We observed a significant reduction in lesion volume at 1, 4, and 14 dpi in KO compared to WT mice (Fig. 2 *A*–*E*). This correlated with reduced BBB permeability, as measured by Evans Blue extravasation (Fig. 2*F*) as early as 6 hours postinjury (hpi). Importantly, KO mice show improved motor recovery at 7 and 14 dpi using rotarod assessment (Fig. 2*G*), which is also consistent with a significant improvement in their acute cerebral blood flow (CBF) at 4 dpi by laser Doppler imaging (Fig. 2 *H* and *J*) compared to WT mice (Fig. 2 *H* and *I*). To identify critical factors that may play a role in mediating tissue protection, RNA was extracted from cortical tissue lysate of *EphA4*$^{f/f}$(WT) and *EphA4*$^{f/f}$*/Tie2-Cre* (KO) mice at 2 hpi and 1 dpi following sham and CCI. Vascular-specific genes and select tight junctions were analyzed by qPCR. We observed that *EphA4* mRNA is significantly up-regulated in the WT mice

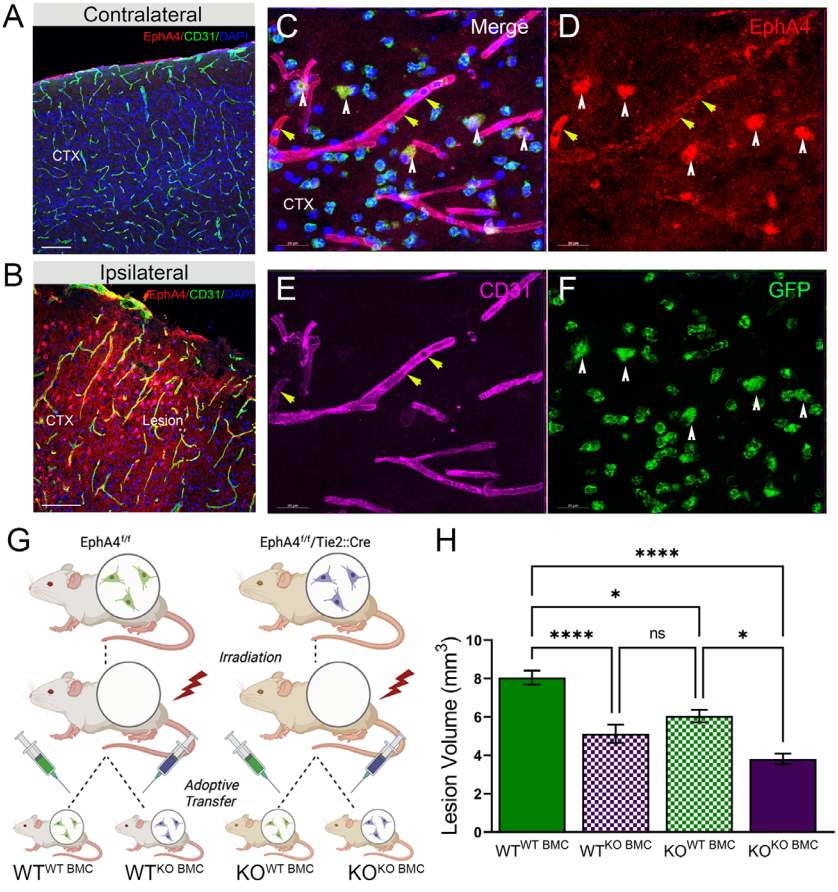

Fig. 1. Bone marrow chimeric *EphA4*$^{f/f}$*/Tie2-Cre* mice show endothelial- and immune-derived EphA4 mediates tissue damage after CCI injury. Representative low-magnification confocal images in the contralateral (*A*) and ipsilateral (*B*) cortex. (*C*–*F*) GFP chimeric mice show EphA4 (*D*) on Cd31-positive microvessels (*E*; yellow arrow head) and GFP-expressing immune cells (*F*; white arrow head) at 1dpi in the ipsilateral perilesional cortex. (*G*) Replacement of bone marrow from *EphA4*$^{f/f}$*/Tie2-Cre* (KO) and *EphA4*$^{f/f}$ (WT) mice with BMCs from *EphA4*$^{f/f}$*/Tie2-Cre/Rosa*^{mTmG} mice (KO$^{KO\ BMC}$ and WT$^{KO\ BMC}$, respectively) or BMCs from *EphA4*$^{+/+}$*/Tie2-Cre/Rosa*^{mTmG} mice (KO$^{WT\ BMC}$ and WT$^{WT\ BMC}$, respectively). (*H*) Quantified lesion volume shows that all conditions are neuroprotective with the greatest benefit in KO$^{KO\ BMC}$ (loss-of-function in both populations). n = 5 to 11 per group. One-way ANOVA Tukey post hoc. *$P < 0.05$, ****$P < 0.0001$.

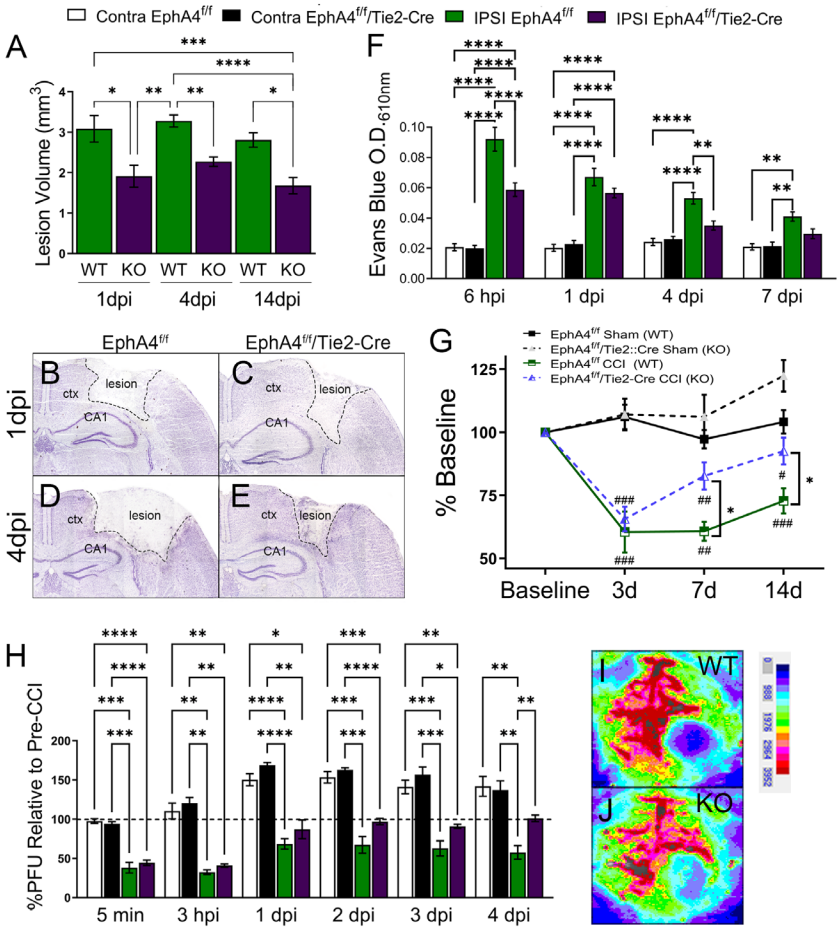

Fig. 2. *EphA4$^{f/f}$/Tie2-Cre* mice display reduced lesion volume, BBB permeability, improved motor function, and cerebral blood flow following CCI injury. (*A*) Quantified lesion volume at 1, 4, and 14 dpi. n = 5 to 13/group. (*B*–*E*) Representative mosaic tiled images of Nissl-stained ipsilateral cortices at 1 and 4-dpi. (*F*) Quantified Evans blue dye in the contralateral (Contra) and ipsilateral (IPSI) cortices at 6 h, 1, 4, and 7 dpi. n = 7 to 11. (*G*) Performance on Rotarod is improved in CCI-injured KO mice compared to CCI-injured WT at 7- and 14-dpi (# significant from the corresponding sham group; *significant between CCI groups). n = 15 to 21/group. (*H*) Laser Doppler quantification of cerebral blood flow (CBF) in perfusion units (PFU) of the ipsilateral cortex. n = 5 to 7/group. (*I* and *J*) Representative images of laser Doppler analysis of CBF. Scale=red-blue, high to low CBF. WT = wild type; KO = knockout. One-way ANOVA Tukey post hoc (*A*); Two-way ANOVA, repeated measures (*F*, *G*, and *H*). *$P < 0.05$, **$P < 0.01$, ***$P < 0.001$, ****$P < 0.0001$.

at 2hpi and *Tjp1, Aqp4, Ocln*, and *Cldn5* were significantly increased in the KO injured cortex at 1dpi (*SI Appendix*, Fig. S1). These findings support a cell-specific role of EphA4 as a negative regulator of tissue damage, BBB gene expression, and functional deficits in brain injury.

Endothelial Cell–Specific Deletion of EphA4 Ameliorates Tissue Damage, Blood–Brain Barrier Permeability, and Functional Motor Deficits Following TBI. To address endothelial cell (EC)–derived EphA4 on the TBI outcome, we subjected *EphA4$^{f/f}$/VE-Cadherin-Cre^{ERT2}* (iKO) and *EphA4$^{f/f}$* (iWT) mice to sham or CCI injury. We found that iKO mice display a significant reduction in lesion volume at 1, 4, and 14 dpi (Figs. 3*A* and 4*B*) compared to iWT mice. A significant reduction in BBB permeability by EB extravasation at 6 hpi and 1 to 7 dpi (Fig. 3*D*) was also observed in the ipsilateral cortex of iKO mice, which was consistent with reduced IgG deposition in the damaged cortex at 1dpi in iKO (Fig. 4 *E* and *G*) compared to iWT (Fig. 3 *E* and *F*). These data comport with findings of increased motor recovery at 7 and 14 dpi (Fig. 3*C*) and altered presence of CD45^{hi} immune cells and CD45^{hi}/CD68 double-labeled cells in the iKO damaged cortex at 2 hpi, 1 dpi and 4 dpi (*SI Appendix*, Fig. S2 *L* and *M*). Additional ultrastructural analysis using TEM further demonstrates that iKO perilesional microvascular display reduced numbers of macropinocytic vesicles (125 to 300 nm), predominant mediators of BBB disruption through increased transcytosis of plasma (23, 24), at 1 dpi (Fig. 3 *I*, *K*, and *L*) compared to iWT (Fig. 3 *H*, *J*, and *L*). These findings demonstrate a role for EC-specific EphA4 in mediating neural tissue damage, motor deficits, and BBB disruption.

Single-Cell RNA Sequencing of Capillary-Specific Endothelial Cells from the Damaged Cortex Shows the Distinct Differential Gene Expression in *EphA4$^{f/f}$/VE-Cadherin-Cre* Mice. The mechanistic role of EC-specific EphA4 was characterized using single-cell RNA sequencing (scRNAseq) from the iWT and iKO injured cortex to test the differential gene expression (DGE) pattern in microvascular endothelial cells. A total of 3,336 cells from iWT and 5,011 for iKO were included for analysis, and libraries were sequenced to a median depth of ~14,000 reads/cell, detected a median of ~3,500 transcripts per cell, and represented a median of ~1,400 genes per cell. SingleR was used to perform unbiased cell type recognition by leveraging the mouse RNAseq database reference of pure cell types to infer each cell origin for each group (Fig. 4*A*). Neural dissociation using papain resulted in predominate capture of endothelial cells, astrocytes, glia, and immune cells. We then performed custom annotations to identify different endothelial cell types in the EC cluster. We stratified EC type by overlaying expression of *Tek, Cdh5*, and *Pecam* with capillary marker *Glut1;* artery marker *ephrinb2*, and venous marker *EphB4* (Fig. 4*B*). The DGE for the capillary-type ECs from iKO mice showed 94 genes that were up-regulated and 54 down-regulated genes (>1.2 FC; <0.05 adj *P*-value) compared to iWT capillary–type ECs (Fig. 4*C*). The heatmap of the top genes shows clear differential expression patterns (Fig. 4*D*). We find *Akap12,* A-kinase anchor protein 12, which serves as a scaffolding protein in signal transduction and involved in vascular integrity (25, 26), to be the highest expressed gene in iKO (1.78 log2FC, adj *P* = 5.19E-22). In addition, *Tmem252* (1.67 log2FC, adj *P* = 1.27E-30), *Colec12* (1.50 log2FC, adj *P* = 1.75E-29), *Phactr4* (1.13 log2FC, adj *P* = 1.54E-15) and *Smad1* (0.99 log2FC, adj *P*

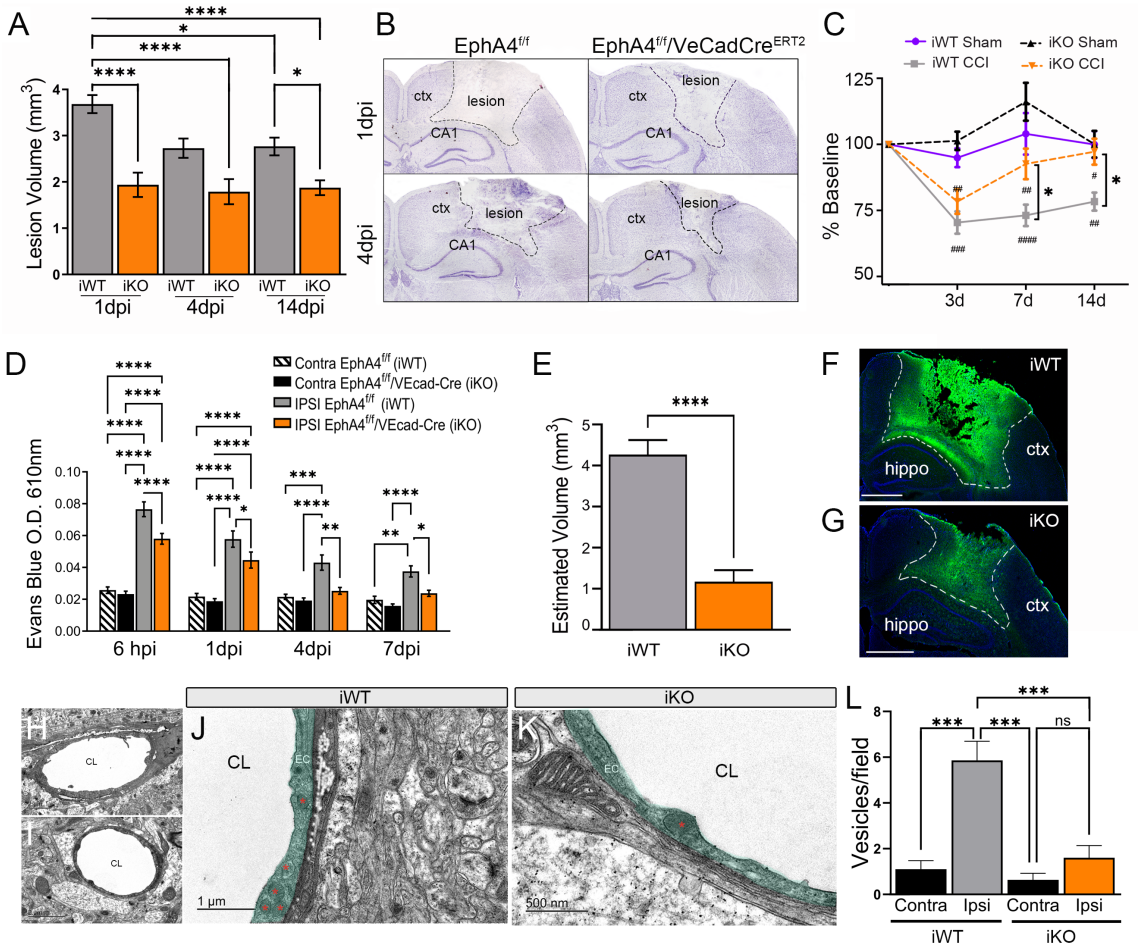

Fig. 3. *EphA4$^{f/f}$/VE-Cadherin-Cre* mice display reduced lesion volume, BBB permeability, improved motor function, and ultrastructural changes following CCI injury. (*A*) Quantified lesion volume at 1, 4, and 14 dpi. n = 5 to 9/group. (*B*) Representative mosaic tiled images of Nissl-stained ipsilateral cortices of iWT and iKO mice at 1 and 4 dpi. (*C*) Performance on Rotarod is improved in CCI-injured iKO mice compared to CCI-injured iWT at 7- and 14-dpi (# significant from the corresponding sham group; *significant between CCI groups). n = 15 to 22/group. (*D*) Quantitative analysis of Evans blue dye at 6 h, 1, 4, and 7 dpi. n = 6 to 11. (*E*) Quantified volume of IgG deposition in perfused coronal serial sections of iWT (*F*) and iKO (*G*) compared to at 1 dpi. (*H* and *I*) Low mag TEM images of capillaries in the perilesional cortex at 1dpi of iWT (*H*) and iKO (*I*). Increased macropinocytosis in iWT depicted by red asterisks (*J* and *L*) compared to iKO (*K* and *L*). Magnification 10,000×; Scale bar, 1,000 nm in *J*; 500 nm in *K*; 2 µm in *H* and *I*. CL = capillary lumen; EC = endothelial cell; –iWT = Tam-injected wild-type; iKO = Tam-injected knockout. One-way ANOVA Tukey post hoc (*A*); Two-way ANOVA (*F–I*). *P < 0.05, **P < 0.01, ***P = <0.001, ****P < 0.0001. (Scale, 1 mm in *F* and *G*.)

= 2.25E-16) were also enriched in iKO cells displaying clear and distinct expression changes by feature maps (Fig. 4*E*).

We categorized the raw average gene expression from capillary-derived ECs for relevant genes involved in BBB function, including Angpt/Tie2, tight junction (TJ)-associated (*Tjp1, Ocln, Cldn5*, and *Akap*12) adheren junction (AJ)-associated (*Ctnnb1, Ptprm*, and *Ppp2r2a*), and related actin cytoskeletal regulators (*Rdx, Msn, Pak2*, and *Arpc3*). Importantly, we find a 60-fold reduction in EphA4 for iKO (0.013) compared to iWT (0.779) (Table 1). Cultured EphA4-deficient endothelial cells displayed a significant increase in mRNA expression of *Ocln, Tie2, Cdh5*, and *Tjp1* when exposed to shear mechanical 106 dyne/cm^2 stress levels (11), compared to WT cells (*SI Appendix*, Fig. S3 *A–D*, respectively), suggesting that mechanical force may in part contribute to EphA4 regulation of vascular gene expression. Collectively, the effects observed on these principal BBB structure-associated genes suggest that EC-specific EphA4 negatively regulates BBB integrity through control of junctional complexes between ECs in response to TBI.

Endothelial Cell Enrichment from *EphA4$^{f/f}$/VE-Cadherin-Cre* Mice Shows Altered mRNA Expression and Changes in the Cortical Transcriptomic Landscape. Validation of the scRNAseq findings was performed by isolating ECs from the ipsilateral cortex of sham and CCI-injured iWT and iKO mice at 1dpi using Cd31-microbeads (Fig. 5*A*). mRNA expression was evaluated using qPCR, and EC identity was confirmed as transcripts for *Gfap, Cx3cr1, Neun, Cd90,* and *Aqp4* were nominally expressed compared to *Tek* (Tie2) (Fig. 5*B*). In addition, transcripts for EphA4 were not detected (nd) in iKO EC samples, confirming its deletion (Fig. 5*C*). CCI-injured iWT ECs showed a significant increase in angiopoietin-2 (*Ang2*), a Tie2 antagonistic, that is significantly attenuated in iKO cells (Fig. 5*D*). In contrast, angiopoietin-1 (*Ang1),* an agonist, is significantly down-regulated in iWT and iKO CCI-injured cells along with *Tie2* and *Occludin* (*Ocln*) (Fig. 5 *E–G*; respectively). Western blot analysis revealed increased protein expression of Cldn5, pAkt (473), Akt, and Akap12 as well as reduced Ang2 in the iKO ipsilateral CCI–injured whole cortex compared to iWT (Fig. 5 *H* and *I*). Finally, whole genome-wide RNA sequencing of the EC-depleted injured cortex (flow-through) showed a significant difference in the number of up- (436) and down-regulated (112) genes in iKO compared to iWT samples (Fig. 5*J*). The 12 genes found to be highly up-regulated in iKO included *Kif5a, Slc6a17, Ppfia3, Rims1, Rph3a, Pcsk1n, Kifc2, Psd, Dlgap2* and *3, Rab15,* and *Tmp1* (Fig. 5*K*). Gene Ontology (GO) of up-regulated (UpReg) DEGs revealed a striking difference in pathways related to the GO terms: synapse,

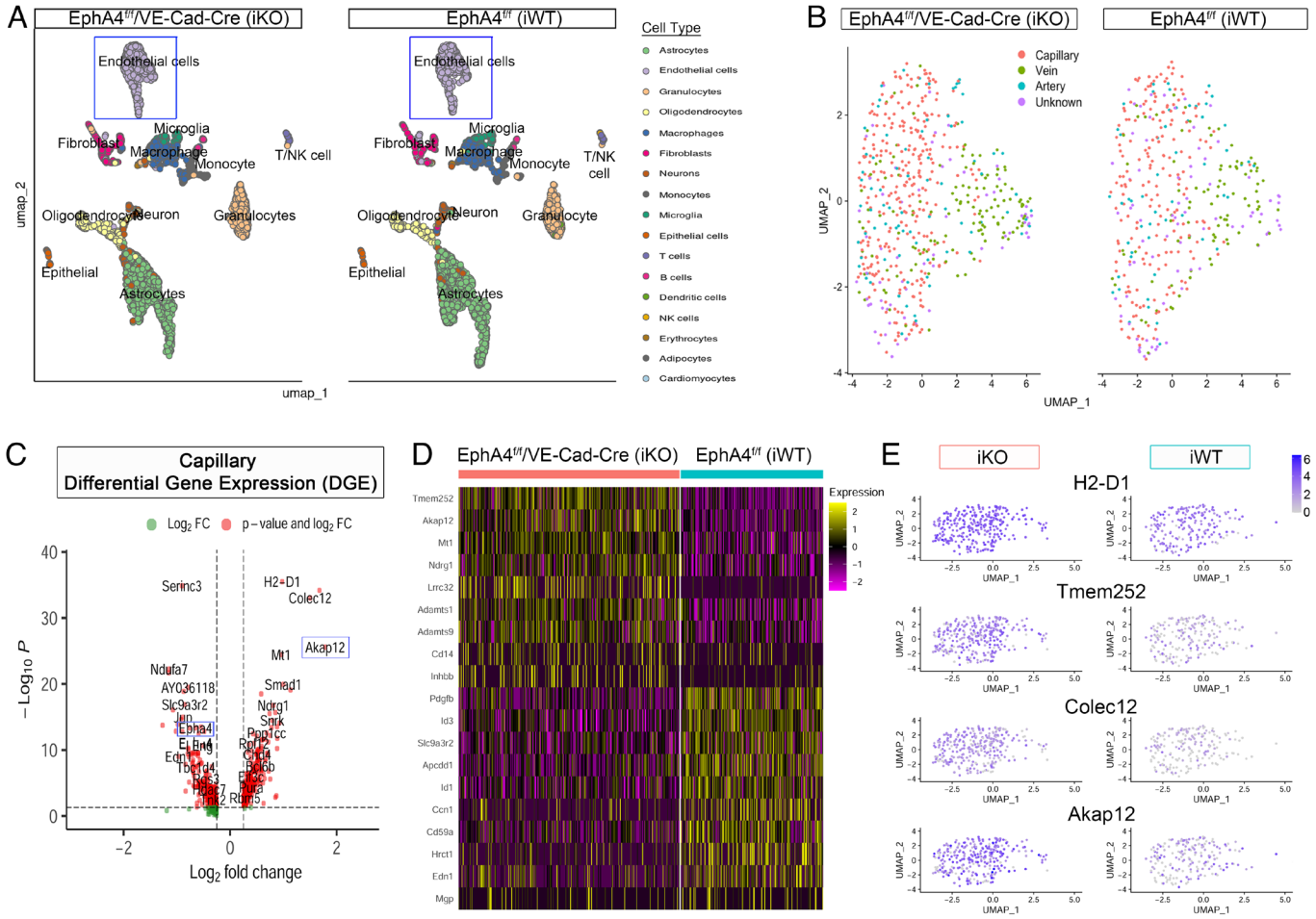

Fig. 4. scRNAseq analysis of the ipsilateral cortex displays differential gene expression in capillary-derived ECs in *EphA4$^{f/f}$/VE-Cadherin-Cre* mice at 1 dpi. (*A*) Cortical cells from iWT and iKO are clustered based on RNA gene expression in a Uniform Manifold Approximation and Projection (UMAP) plot. (*B*) ECs were further classified as capillary-, artery-, or vein-derived using custom annotation. (*C*) Volcano plot showing significant genes vs. log2Fold change. *EphA4* was among the down-regulated, and *Akap12* was up-regulated in iKO cells (*D*) Heatmap of top DEG's (*Y* axis) per cluster (*X* axis) for iWT and iKO showing distinctive gene expression profiles between capillary-derived ECs. Yellow and purple represent higher and lower gene expression, respectively. (*E*) Feature plots UMAP visualization overlaid with the expression of selected up-regulated genes *H2-D1, Tmem252, Colec12, and Akap12* in iKO cells.

synaptic transport, ion channel transport, and negative regulation of neuron apoptosis (Benjamini–Hochberg adjusted *P*-value < 0.05) (Fig. 5*L*). These findings suggest that loss of EphA4 function in ECs influences gene pathways related to neuronal health and signaling in the cortex following CCI injury.

Tie2 Receptor Inhibition Attenuates BBB Integrity, *Akap12* and *Cldn5*, and Neuroprotection in *EphA4$^{f/f}$/VE-Cadherin-Cre* Mice. Differential expression from scRNAseq, qPCR, and western blot identified *Akap12* as highly expressed in iKO capillary ECs compared to iWT. Evidence suggests that Akap12 maintains endothelial cell integrity, controls cell–cell adhesion, and regulates tight junction protein expression via Ang1 (27, 28). To test the role of Tie2 function on *Akap12* expression, BBB permeability, and tissue damage in the absence of EC-specific EphA4, we treated iWT and iKO mice with 1 mg/kg soluble recombinant (s)Tie2-Fc or Fc-control immediately following CCI injury. We find that iKO mice that received sTie2-Fc failed to exhibit neuroprotection (Fig. 6 *A* and *F*) as seen in Fc-control treated iKO mice (Fig. 6 *A* and *D*) and showed a similar lesion volume as iWT mice that received either Fc-control or sTie2-Fc at 1 dpi (Fig. 6 *A*, *C*, and *E*, respectively) at 1 dpi. Tie2 inhibition in iKO mice also showed attenuation of BBB protection (Fig. 6*B*). Isolation of cortical-derived ECs under these conditions confirmed that control iKO ECs displayed a fivefold increase in *Akap12* and *Cldn5* mRNA levels compared to iWT and that Tie2 inhibition significantly attenuated these effects (Fig. 6 *G* and *H*, respectively). A similar trend in *Ocln* was observed but did not reach statistical significance compared to iWT Fc-control (Fig. 6*I*). Immunohistochemistry further shows that the number of Tie2-positive vessels expressing Akap12 protein in the ipsilateral dorsal cortex of iKO was significantly increased (Fig. 6 *Q*–*T*) compared to iWT (Fig. 6 *M*–*P*), and as quantified by the number of vessels expressing Akap12 (Fig. 6*U*). Notably, the number of ipsilateral vessels expressing Akap12 was attenuated in iKO mice treated with sTie2-Fc. Colocalization of Akap12 with Tie2 clusters is also enhanced in the iKO ECs (Fig. 6 *T*, *Inset*, yellow) compared to iWT (Fig. 6 *P*, *Inset*, yellow). Last, few vessels in the contralateral cortex expressed Akap12 (Fig. 6*V*), suggesting that its expression can be induced by injury but is limited by EphA4 signaling via the Tie2 receptor.

Last, to directly test the functional role of Tie2 in CCI-induced damage, we stimulated Tie2 using the angiopoietin-1 mimetic peptide Vasculotide at 150 μg/kg i.v. injection (29) following CCI injury. At 1 dpi, we observed a significant reduction in lesion volume in VT-treated mice (Fig. 6 *K* and *L*) compared to vehicle-treated (Fig. 6 *J* and *L*). These results demonstrate that EphA4 mediates tissue damage by suppressing Akap12/Tie2

Table 1. Raw average gene expression values from all capillary-derived endothelial cells

Genes	(1) iKO	(2) iWT	Protein name	Function
EphA4	*0.13189004	0.77889278	EPH receptor A4	Axon growth and guidance
Angpt/Tie2 pathway				
Tek	2.23146166	1.87926998	Tie2 receptor	RTK, a receptor for angiopoietins; BBB integrity
Angpt1	0	0	Angiopoeitin-1	Vascular protective: suppress plasma leakage, inhibit vascular inflammation, and prevent EC death
Angpt2	0.94411612	1.21736127	Angiopoeitin-2	Stored in EC Weibel-Palade bodies; acts as a Tek antagonist; EC activation, destabilization, and inflammation
Tight junctions or TJ-associated				
Tjp1	3.84163701	4.14777154	Zonula occludens 1	Tight junction protein
Ocln	1.86946376	2.24117737	Occludin	Tight junction protein
Cldn1	0	0	Claudin-1	Constituents of tight junction complex
Cldn5	59.5056848	56.370172	Claudin-5	Constituents of tight junction complex
Akap12	*15.9917638	3.93422676	A-kinase anchoring protein 12	Supports BBB Integrity; Zo-1/Claudin5 expression; essential for the integrity of the endothelium via Pak2 and AF6
Adheren junctions or AJ-associated				
Ctnnb1	*6.25670823	4.77784115	β-catenin	Component of cadherin protein complex
Ptprm	*1.10660973	0.66690377	Protein tyrosine phosphatase receptor type M	VE-cadherin/catenin complex; regulation of shear stress mechanotransduction
Ppp2r2a	*1.03698102	0.65053351	Protein Phosphatase 2 regulatory subunit Balpha	Associates with b-catenin; TJ trafficking
Actin cytoskeletal regulators and ERM (Ezrin/radixin/Moesin)				
Rdx	*4.06813477	3.01084394	Radixin	Cytoskeletal protein linking actin to plasma membrane
Msn	*9.19652056	7.29732442	Moesin	Cytoskeletal protein linking actin to plasma membrane
Pak2	*2.69915355	1.70900812	P21 (RAC1) Activated Kinase 2	Actin cytoskeletal regulator, Regulated by Akap12
Arpc3	*8.38355483	6.8099543	Actin-Related Protein 2/3 Complex Subunit 3	Control of actin, Cadherin/catenin complex-mediated endothelial cell–cell adhesion and integrity

*Single-cell data (pct.) show significant DGE changes in iKO compared to iWT. <0.05 *P*-value.

receptor signaling, a target for neuroprotection, in a murine model of focal cortical impact.

Human Serum Expression of Angiopoeitin-2 Is Enhanced in Moderate/Severe TBI Patients. Angiopoietin 2 is a vascular-specific protein that has been implicated in BBB disruption (30, 31) and is attenuated in the absence of EphA4 in our mouse model. To investigate the association of human TBI with angiopoietin-2 expression over time, a linear mixed model was developed and used to analyze male serum samples. No differences in age or race across TBI and control samples were seen (Fig. 7*A*; $P = 0.829$, $P = 0.637$). Using ELISA, we evaluated protein expression from serum collected at <24 h (time of admittance), 48 h, and 72 h. We observed a significant increase in expression at <24 h and 48 h (Fig. 7 *B* and *C*; $P = 0.009$, $P < 0.001$, respectively), which was not statistically significant at 72 h ($P = 0.168$). Further, our pilot study shows that the increase in Ang2 expression may correlate with injury severity as observed in patients with GCS <8 at 24 and 48 h (Fig. 7 *I* and *J*; respectively) and in GCS 9-12 at 48 h and 72 h (Fig. 7 *J* and *K*, respectively). These data emphasize the potential clinical relevance of targeting Ang/Tie2 signaling acutely following TBI and suggest that markers related to this pathway may serve as diagnostic biomarkers.

Discussion

Traumatic brain injury remains a leading cause of injury-related death and disability worldwide and is a significant contributor to the sequela of other comorbidities. Importantly, understanding the BBB response is an important focus area aimed at uncovering the underlying cause of acute and progressive tissue damage following trauma. The current study utilized both a chimeric and conditional gene-targeted approach to assess the cell-autonomous role of EphA4 in regulating CCI injury outcomes. Our current tissue expression analysis revealed the upregulation of EphA4 on microvessels and infiltrating immune cells. While our prior findings observed EphA4 expression on microglia, its gene deletion using conditional $EphA4^{f/f}/Cx3cr1^{CreERT2}$ mice showed no effect on tissue outcome (32) and, at the same time, global loss of EphA4 displayed neuroprotection (18). Here, we reveal that tissue protection is gained from peripheral immune-specific deletion of EphA4 and that conditional knockout in endothelial cells (ECs) also results in significant neuroprotection and functional recovery. Uniquely, we showed that the effect of gene deletion in ECs coincides with reduced BBB disruption and increased expression of tight junction complex gene *Cldn5,* and TJ-associated *Akap12*, while a difference was found in *Ocln* or *Tjp1*. Furthermore, the BBB integrity, *Cldn5* and *Akap12* expression, and tissue protection

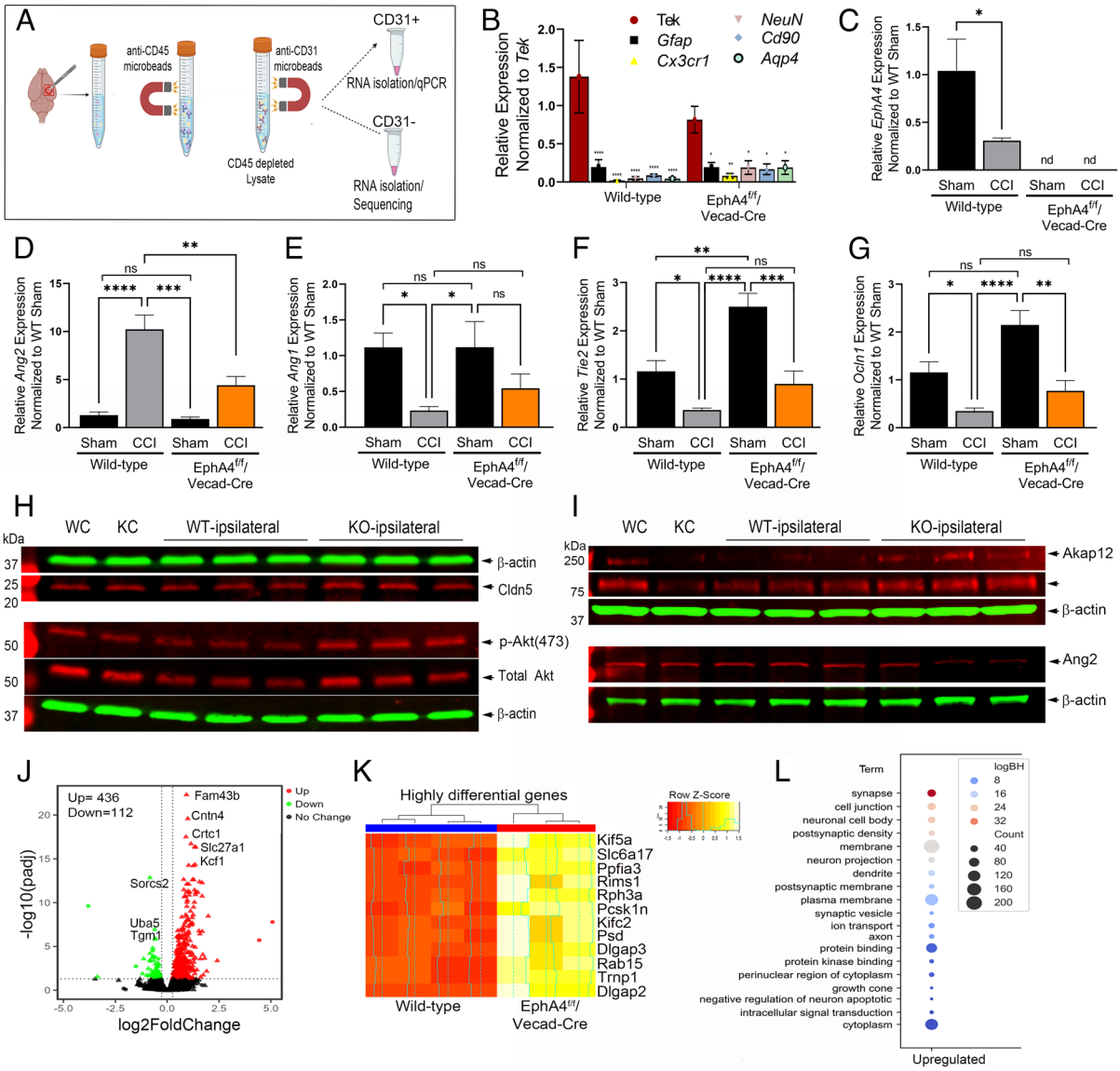

Fig. 5. Altered gene expression of Cd31-microbead sorted ECs and whole genome-wide RNAseq of the injured *EphA4$^{f/f}$/VE-Cadherin-Cre* cortex. (*A*) Graphical representation of the experimental design for the endothelial cell (EC) enrichment using Cd31-microbeads. (*B*) ECs isolated from *EphA4$^{f/f}$/VECad-Cre^{ERT2}* iKO and *EphA4$^{f/f}$* iWT show enrichment for *Tek* (Tie2) compared to *Gfap, Cx3cr1, Neun, Aqp4*, and *Cd90*. (*C–G*) Quantitative mRNA analysis of the EC fraction showing *EphA4* (*C*), *Ang2* (*D*), *Ang1* (*E*), *Tie2* (*F*), and *Ocln1* (*G*). (*H* and *I*) Western blot analysis for Cldn5, pAkt, Akt, Akap12, Ang2, and β-actin expression in the iWT contralateral (WC), iKO contralateral (KC) and iWT, iKO ipsilateral cortex at 1 dpi. (*J*) Volcano plot showing statistically significant genes (−log10padi) versus magnitude of change (log2Fold Change). (*K*) The top 12 highly differential genes included genes involved in synapse and ion channel function, including *Kif5, Psd, Dlgap,* and *Slc6a17*. (*L*) Gene Ontology (GO) analysis of the 436 up-regulated genes confirmed that the gene clusters were related to the synapse, synaptic transport, ion channel transport, and negative regulation of neuron apoptosis. One-way ANOVA Tukey post hoc. *$P < 0.05$, **$P < 0.01$, ***$P < 0.001$, ****$P < 0.0001$. ns = not significant.

are lost when Tie2 was inhibited in *EphA4$^{f/f}$/VE-Cadherin-Cre* but not in wild-type mice. These findings provide mechanistic insight into the cell-autonomous role of EphA4 as a critical mediator of BBB permeability via suppressive control over Tie2/Akap12 signaling to regulate tissue damage following TBI.

The brain endothelium has highly enriched levels of tight junction proteins (TJPs) such as occludin, claudin (Cld 3, 5, and 12), zonula occludens proteins (ZO-1, -2), and junctional adhesion molecules which make it unique from other endothelium (33). Barrier integrity and regulation of tight junctions are vital for proper BBB function. However, our understanding of how mechanical injury and the secondary biochemical changes that occur following trauma affect TJPs remains unclear. Using Evan's blue dye, we find increased extravasation into the brain after CCI injury, which was attenuated in the absence of EC-specific EphA4. This effect coincides with increased TJ mRNA expression in vivo and in vitro. Simulation of mechanical stress on WT and KO cultured ECs also demonstrates that EphA4 may restrict the expression of TJ genes under certain conditions. At present, it is unclear which ephrin ligand is responsible for endothelial-EphA4 activation and subsequent BBB disruption after CCI injury. EphrinB2 has been shown to be up-regulated on microvessels and perivascular support cells after stroke, and its activation via EphB4 can protect the BBB (34). EphA2 mediates BBB breakdown during *Plasmodium* infection, in part through its high-affinity binding partner ephrinA1 (35), which EphA4 is also known to have high-affinity binding (36). Given that the EphA4 receptor is capable of binding multiple class A and B ligands, an extensive analysis of ephrin binding and function in the brain microvascular niche is needed.

Administration of soluble ectodomain Tie2-Fc blocked the beneficial effects on tissue and BBB protection, demonstrating EphA4's

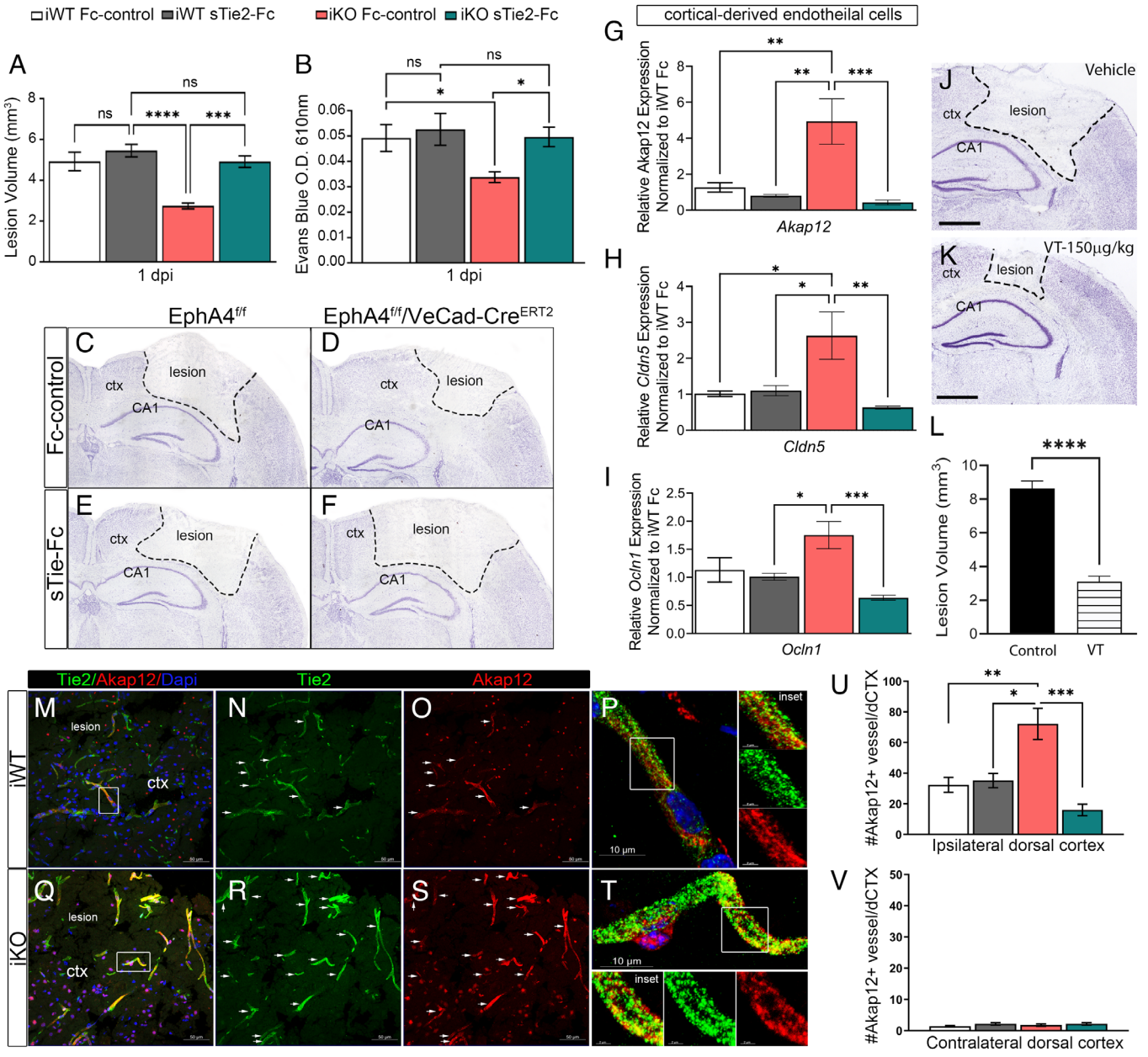

Fig. 6. Tie2 inhibition attenuates neural tissue, BBB protection, and Akap12 expression in *EphA4$^{f/f}$/VE-Cadherin-Cre* mice at 1dpi. (*A*) Quantified lesion volume as calculated from serial sections spaced 300 µm apart shows iKO receiving recombinant soluble (s)Tie2-Fc intravenously immediately following CCI injury showed attenuation of protection when compared to iKO mice receiving Fc-control at 1dpi. (*B*) Evans blue dye of iWT and iKO ipsilateral cortices shows a reduction in extravasation in iKO Fc-control treated mice that are attenuated when iKO mice were treated with sTie2-Fc. *$P < 0.05$ compared to iWT Fc control, n = 6 per group. (*C–F*) Representative Nissl-stained mosaic-tiled images at 4× magnification. (*G–I*) ECs were microbead isolated from the ipsilateral cortex at 1dpi, and qPCR shows that mRNA levels of *Akap12* (*G*) and *Cldn5* (*H*) were significantly increased in iKO-Fc but attenuated in iKO sTie2-Fc-treated mice. (*J–L*) Administration of vehicle (*J*) or Vasculotide (VT; *K*) at 150 µg/kg shows reduced lesion volume as calculated from serial sections spaced 450 µm apart (*L*). (*M–P*) Immunohistochemistry of Tie2-positive vessels (green), Akap12 (red) in iWT damaged cortex and (*Q–T*) expression in iKO at 1dpi. (*U*) Quantification of the number (#) of Akap12+/Tie2+ vessels in the ipsilateral cortex. (*V*) Few Akap+/Tie2 vessels found in the contralateral cortex. One-way ANOVA Tukey post hoc. *$P < 0.05$; **$P < 0.01$, ***$P < 0.001$, ***$P < 0.0001$. Scale, 50 µm *M–O*; and *Q–S*, 0.5 mm *J* and *K*; Scale, 10 µm in *P* and *T* and Scale, 2 µm *Insets*. ns = not significant.

influence over the Tie2 signaling. Tie2 has been shown to regulate tight junction molecule expression (37, 38), and following angiopoietin-1 activation, it promotes vascular stability and can reduce vascular leakage (39). Moreover, angiopoietin-2 (Ang2) may function to antagonize Tie2, and Ang2-blocking antibodies can reduce inflammation-associated vascular leakage (40). Interestingly, we find that *Ang2* mRNA levels are up-regulated on injured cortical iWT ECs. This effect is attenuated in ECs isolated from iKO mice coinciding with reduced Ang2 protein expression in the damaged cortex, which could lead to enhanced Tie2 activation resulting in improvements in TJ expression and BBB protection. This may explain why Tie2 inhibition reversed the observed effects in iKO but not iWT mice. We further show that Vasculotide, an angiopoietin-1 mimetic that directly stimulates Tie2 and protects against vascular leakage in abdominal sepsis, kidney injury, and hemorrhagic shock (29, 41–43), is neuroprotective in TBI. These findings suggest that Tie2 stimulation may be a key target for neurovascular protection in the brain. Indeed, our clinical findings demonstrate a significant increase in the Ang2 ligand, a Tie2 antagonist produced primarily by endothelial cells (40, 44), in human patients <24 h following moderate/severe TBI. This suggests that Ang2 levels in the serum may be diagnostic of

A

Variables	TBI	Controls	P value
Age (mean ± SD)	26.6 ± 9.4	25.8 ± 12.1	0.829
Race			0.637
Asian	1 (5.6%)	0 (0%)	
Black	5 (27.8%)	2 (15.4%)	
Hispanic	1 (5.6%)	0 (0%)	
White	11 (61.1%)	11 (84.6%)	

B

Predictors	Estimates	CI	p
Intercept	0.68	-0.02 – 1.37	0.055
<24 hours	1.65	0.59 – 2.72	0.009
48 hours	2.17	1.10 – 3.24	<0.001
72 hours	1.04	-0.03– 2.11	0.168
δ^2	0.77		
τ_{00} subject	1.37		
ICC	0.64		
$N_{subject}$	31		
Observations	57		
Marginal R^2 / Conditional R^2	0.254 / 0.730		

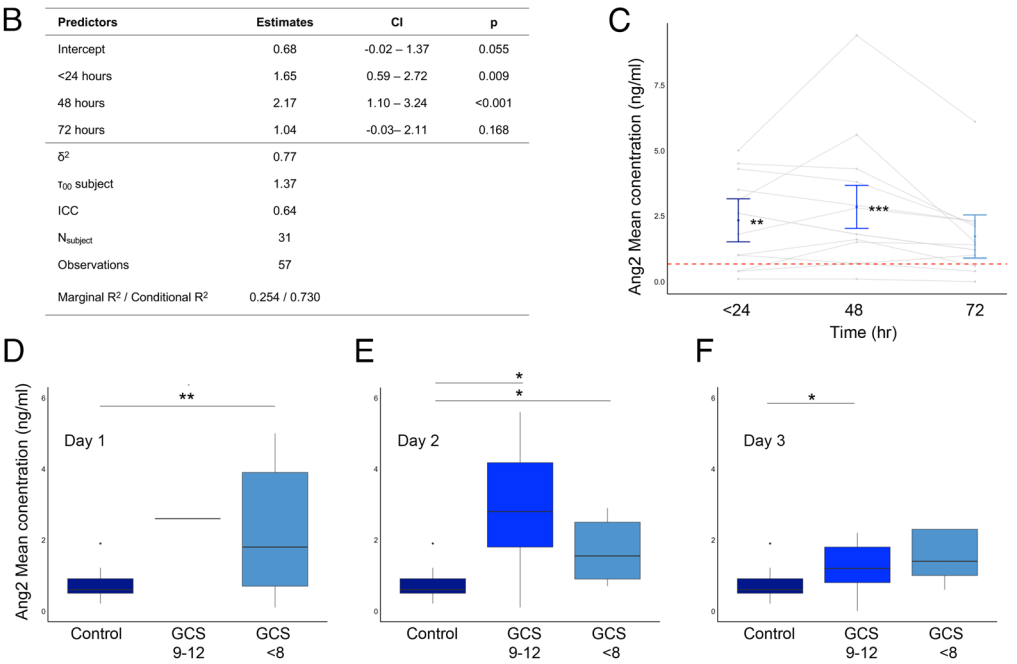

Fig. 7. Analysis of angiopoietin-2 (Ang2) in human serum following acute TBI. (*A*) Patient demographics show no difference in age or race across TBI and control patients for male subjects. (*B* and *C*) Measurement of serum protein Ang2 in male TBI patients demonstrates significant elevation at <24 h and 48 h posthospital admission. The red dashed line represents the mean concentration value for control sera. The model includes time as a fixed effect, a random intercept for subject. (*D–F*) Following hospital admission, severe male TBI patients (GCS <8) exhibit elevated Ang2 values (ng/mL), while moderate (GCS 9-12) patients exhibit elevated Ang2 levels at 48 and 72 h post-TBI. A linear mixed effects model for serial Ang2 expression was used. ANOVA for comparison with TBI severity. Bonferroni post hoc correction was utilized for all tests. **P* < 0.05; ***P* < 0.01, ****P* < 0.001, ****P* < 0.0001.

severity and/or support clinical analysis of BBB evaluation. Future studies may also focus on the association between angiopoietin expression and chronic functional outcome status.

Single-cell RNAseq was performed on cortical tissue in order to resolve transcriptomic changes specific to capillary-derived ECs in response to CCI injury. We uniquely identified Akap12, A-kinase anchor protein12, to be highly expressed in iKO capillary–ECs. Akap12 is a scaffolding protein that associates with specific complexes to improve the spatiotemporal function of intracellular signal proteins (28). It supports barrier function in fibrotic scars (45), vascular integrity in zebrafish (46), blood-retinal barrier (27), and BBB integrity in ischemic stroke where EC loss of Akap12 mediates dysregulation of Cldn5 expression (25). Akap12 signalosome is recruited to the plasma membrane in myocytes and binds to β-AR to help compartmentalize PKA signaling (47). Our high magnification confocal image analysis suggests that loss of EC-specific EphA4 may enhance the recruitment of Akap12 to Tie2 clustering domains in the microvessels of the damaged cortex. This mechanism may potentially enhance Tie2 signaling and promote barrier integrity through downstream regulation of junctional protein complexes (38, 48). Indeed, our scRNAseq (Table 1) shows that iKO capillary–derived ECs show a significant increase in adheren junctions (AJ) (*Ctnnb1, Ptprm*), AJ-associated (*Ppp2r2a*), and actin cytoskeletal regulators (*Rdx, Msn, Pak2*, and *Arpc3*). *Akap12* mRNA expression is also directly regulated by Tie2 signaling in iKO ECs. Further studies are needed to meticulously probe the nature of the spatial interaction between Akap12 and the Tie2 receptor. We further observed increased Akap12 protein expression in the damaged cortex, and on microvessels in the per-lesion of iKO mice which coincided with increased pAkt, Akt, and Cldn5 expression. Protecting the BBB by targeting these key pathways may also benefit the injured environment. Our bulk sequencing data from the cortex revealed significant modulation of genes involved in neuronal function and health. The up-regulated DEGs were enriched for crucial genes involved in synapse and ion channel function, including *Kif5, Psd, Dlgap,* and *Slc6a17*, which regulate vesicular axonal transport (49), microtubule binding (50), synapse organization (51), and synaptic vesicle membrane flow (52).

In conclusion, this work uncovered a contribution of EphA4 to secondary injury by negatively regulating EC function resulting in BBB disruption, neural tissue damage, motor deficits, and loss of cerebral blood flow. It was demonstrated that EphA4 uniquely orchestrates this by restricting Tie2 receptor signaling and that Akap12 may play a role in this pathway. Detection of Tie2 antagonist, Ang2 at high levels in the serum of patients with TBI, represents a potential biomarker for vascular damage and highlights the therapeutic utility of targeting Tie2 to treat acute TBI. Overall, these findings provide mechanistic insights into the pathophysiology of TBI and mediators of blood–brain barrier regulation.

Methods

Animals. All mice were housed in an AAALAC-accredited facility as described (53). Male *EphA4*$^{f/f}$, *EphA4* $^{f/f}$*/Tie2-Cre*, and *EphA4* $^{f/f}$*/VE-Cadherin-Cre*^{ERT2} on the CD1 background were used for experimentation at 8 to 10 wk of age. Donor report-er

mice, *EphA4* $^{f/f}$*/Tie2-Cre/Rosa26*^{mTmG}; *EphA4*$^{+/+}$*/Tie2-Cre/Rosa26*^{mTmG} were age-matched. All experiments were conducted under Virginia Tech IACUC, #21-044.

Human Study Design. We conducted a prospective pilot study at Carilion Clinic of 15 consecutive patients with moderate-severe TBI between April 2022 and April 2023. The full study was approved by Virginia Tech's IRB #19-470. Legally authorized representatives provided written informed consent. Subjects aged 18 to 50 y had labs drawn at <24, 48, and 72 h following hospital admission. Control samples were purchased to match age, sex, and race (Discovery Life Sciences). ELISAs were conducted on serum samples to quantify Ang2 expression according to the manufacturer's instructions (Boster Bio).

Tamoxifen Administration. Adult male *EphA4* $^{f/f}$ and *EphA4* $^{f/f}$*/VE-Cadherin-Cre*^{ERT2} mice at 8 wk of age were intraperitoneally (i.p.) injected with Tamoxifen (Sigma Aldrich) at a dose of 50 mg/kg for 5 consecutive days. Two weeks following administration, genotyping was performed to confirm Cre expression and EphA4 flox excision using 5 primer system (*SI Appendix*, Fig. S1).

Microbead Isolation of Endothelial Cells. Endothelial cells were isolated from the lesioned cortex using Cd31 microbeads, as we previously described (22). Four mice were pooled per group, and a single-cell suspension was prepared. The suspension was first subjected to CD45-microbeads and column separation (MACS; Miltenyi Biotech) to deplete immune cells. Endothelial and flow-through fractions were resuspended in TRIzol and prepared for RNA isolation, qPCR, and RNA sequencing. Technical triplicates of each pooled sample were used for qPCR.

Controlled Cortical Impact (CCI) Injury and Motor Function Analysis. Male mice were anesthetized with premixed ketamine (100 mg/kg) and xylazine (10 mg/kg) cocktail via subcutaneous injection and positioned in a stereotaxic frame, and CCI was performed as previously described (18) using Φ = 3-mm round tip connected to an eCCI-6.3 device (Custom Design & Fabrication, LLC) at a velocity of 5.0 m/s, depth of 1.8 mm ± 0.05 mm, and 150-ms impact duration. Sham animals underwent craniotomy only. For soluble Tie2-Fc experiments, mice were immediately injected with 100 μL of soluble Tie2-Fc (200 μg/mL; SinoBiological, Inc.) or Fc control (200 μg/mL; SinoBiological, Inc.) via i.v. tail vein injection. Mice were subjected to rotarod as previously described (11).

Peptide Synthesis and Administration of Vasculotide. The tetrameric Vasculotide peptide (29, 54), with an abbreviated structure, HHRHSFK (HHHRHSF) GGGGGK(GGGGGK(HHHRHSF)HHHRHSF) was synthesized without the four-armed PEG, on a Liberty1 microwave-assisted peptide synthesizer (CEM) using solid-phase peptide synthesis (SPPS) via standard fluorenylmethoxycarbonyl (Fmoc) protocols. Synthesis was carried out using Fmoc-Lys(Mtt)-OH as the branching unit and GGGGG as a spacer. In brief, Fmoc-Lys(Mtt)-OH was first added to the resin using HBTU as the coupling agent. The resin was then treated with 20% piperidine in DMF to remove the Fmoc group, followed by 1% TFA/2% triisopropylsilane (TIPS) in CH2Cl2 to remove the Mtt group. Next, five consecutive G residues were added to the peptide N terminus and the K ε-amine to form two GGGGG branches (one on the main chain and one on the branch from the ε-amine on the K residue). Next, Fmoc-Lys(Mtt)-OH was added to each branch. After deprotecting the Fmoc and Mtt groups as detailed above, HHHRHSF was added stepwise via SPPS to each branch, four equivalents per coupling step, to form the tetrameric peptide. After cleavage and isolation, the crude peptide was dissolved in water containing 0.1% trifluoroacetic acid (TFA) and filtered through a 0.45-μm polytetrafluoroethylene (PTFE) filter before purification by preparative RP-HPLC using an 1260 Infinity HPLC system (Agilent Technologies) (*SI Appendix*, Fig. S3). Separations were performed using an Agilent PLRP-S column (100 Å, 10 μm, 150 ×25 mm) monitoring at 220 nm. The expected mass was confirmed using MALDI-TOF, 4800 MALDI TOF/TOF, AB Sciex (*SI Appendix*, Fig. S4). Fractions containing pure products were combined and lyophilized (FreeZone −105 °C, Labconco) and then stored at −20 °C. Immediately following sham or TBI injury, mice were injected with 150 μg/kg of Vasculotide or saline via i.v. tail vein injection.

Blood–Brain Barrier Permeability Analysis and TEM. We measured BBB as previously described (53). Briefly, a 2% sterile Evans Blue (EB, Sigma E2129) solution was i.v tail vein–injected (4 mL/kg of body weight), and 3 h postinjection, cortices were dissected and incubated in 500 μL Formamide (Invitrogen, 15515-026) at 55 °C and absorbance measured at 610 nm (Synergy HTX, multimode reader, BoiTek). Anti-mouse IgG 488 (ThermoFisher) was applied to serial perfused coronal sections, and the area of IgG staining was quantified using a Cavalieri probe, StereoInvestigator. For TEM, mice were perfused with glutaraldehyde (2%) and 2% paraformaldehyde buffer (Bioworld, 30450005-2). The brains cut 1 mm × 1 mm pieces medial and lateral to the core perilesion and processed with osmium tetroxide and en bloc with uranyl acetate. Grid sections were poststained with uranyl acetate. High magnification images at 20,000× or greater were used to evaluate macrocytic vesicles. We imaged ~60 capillary lumens per hemisphere per mouse and report macrovesicles per field at high magnification in two mice per condition.

Evaluation of Lesion Volume. Lesion volume (mm^3) in the ipsilateral cortex was measured using Cavalieri, StereoInvestigator (MicroBrightField) using an upright Olympus BX51TRF motorized microscope (Olympus America) as previously described (18, 32). Analysis was performed blindly using five serial coronal sections spaced 10 slices apart (−1.1 to −2.3 mm A/P from bregma) at 30 μm in Fig. 2–7*A* or spaced 15 slices apart (−1.1 to −2.9 mm A/P) in Figs. 1 and 7 *J*–*L*. Data are represented as the volume of tissue damage (mm^3).

Immunohistochemical Analysis. Serial coronal sections were rinsed with 1X PBS and then blocked in 2% cold water fish skin gelatin (Sigma, Inc.) and 0.2% Triton-X100 for 2 h. Slides were incubated with the primary antibody in block solution overnight at room temperature, rinsed with 1× PBS, incubated with secondary antibody, and mounted with media containing DAPI counterstain (SouthernBiotech). Rabbit anti-EphA4 (Proteintech), goat anti-Cd31 (BD Biosciences), rabbit anti-CD45 (Cell Signaling Technology), rat anti-CD68 (Invitrogen), rabbit anti-Akap12 (Alomone, Jerusalem), and goat anti-Tie2 (R&D Systems). The secondaries used were all raised in donkey (ThermoFisher, USA). Image acquisition was performed using the Zeiss 880 confocal microscope (Carl-Zeiss).

Quantitative Real-Time PCR. RNA was isolated per manufacturer instructions using TRIzol® reagent (Ambion), then treated using DNAse I (Sigma Aldrich, St. Lois, MO) and quantified using spectrophotometer ND-1000 (NanoDrop). Reverse transcription to cDNA was performed using the iScript™ cDNA synthesis kit (Biorad) per manufacture. For qRT-PCR analysis, 1 μg cDNA per reaction was amplified using iTaq™ Universal SYBR® Green Supermix (Biorad). Changes in expression were analyzed using ΔCq values with reference to the internal control gene *Gapdh*. Relative expression was calculated by normalizing the change in expression to WT levels for each gene. All primers were tested for efficiency ranging from 80 to 110%. Primers sequences (5′-3′) were as follows: Ang1: Fw: CGAAAGCTGACAGATGTTGAGA and Rv: TTTGTCTGTTGGAGAAGTTGCT; Ang2: Fw: GGAAAAGCAGATTTTGGATCAG, Rv: TTCTGCTCCTTCATGGACTGTA; Aqp4: Fw: TCAC ACCTCCCAGTGTGGTT Rv: TGGAATCACAGCTGGCAAAAA; Cldn5: Fw: ATGCAGTGCAAGG TGTATGAAT, Rv: CCGGTCAAGGTAACAAAGAGTG; EphA4: Fw: AAAAATGTACTGTGGGG CAGAT, Rv: TCCGTGGAAAGAGCTTTGTAAT, Gapdh: Fw: CGTCCCGTAGACAAAATGGT, Rv: TCAATGAAGGGGTCGTTGAT; Ocln: Fw: TGGATCGGTATGATAAGTCCAA, Rv: CATAGTCAGATG GGGGTGGAG; Tie2: Fw: AAATGACCCTAGTGAAGCCAGA, Rv: GTCAGGAGGTAAGACTG CGTTG; Tjp1: Fw: TTGGCCAGCCATATATTTGTAAAG, Rv: TTTCCGAGGCATTAGCAGAA; VCAM: Fw: GGTGTACGAGCCATCCACAG, Rv: ACTTGTGGAAATGTGCCCGA; *Akap12*:. Fw: GAAT CCTAAGACGTGAGTTGCT, Rv: CATTGGACGGCTCTGCTCTC.

RNA Sequencing Analysis. The sequencing quality of raw reads was first assessed using FastQC (https://www.bioinformatics.babraham.ac.uk/projects/fastqc/). Using TrimGalore (https://www.bioinformatics.babraham.ac.uk/projects/trim_galore/), reads which passed a mean quality filter of 30 and with lengths greater than 30 were retained for downstream analysis. Clean reads were then mapped to the GRCm38 mouse genome, and gene-level counts were quantified using STAR. Differential expression analysis was performed using DESeq2 (55). Gene Ontology (GO) analysis was performed using DAVID (56, 57), selecting Cellular Compartment (CC), Molecular Function (MF), and Biological Process (BP) terms. Significance values were reported as Benjamini–Hochberg adjusted *P*-values.

Single-Cell Sequencing, Library Generation, and Gene Ontology Enrichment. A 4- × 4-mm piece of injured cortical tissue was neural dissociated using papain digest (Miltenyi Biotec) and cryopreserved in 1 mL of CryoStore® CS10 media (Stem cell technologies). ScRNAseq libraries were generated (Medgenome) using 10× Genomics and sequenced on a NovaSeq 6000 (Illumina). Alignment of the libraries and read counts were performed using Cell Ranger V7.0 (10X Genomics) using Mouse RNA-Seq Database as a reference. Quality control and analysis were done using Seurat

(V 4.1.0 Read10X function) (58). Genes that are not expressed in at least three cells and do not have a minimum 200 expressed genes were excluded, and we filtered for doublets (DoubletFinder package, v2.0.3). The global-scaling normalization method "LogNormalize normalized data" and Seurat were used for clustering. Unbiased cell type recognition using SingleR leveraged reference transcriptomic datasets to independently infer cell origin. The following endothelial markers were used for the identification of capillary (Cd31, Tie2, Cdh5, and Glut1), artery (Cd31, Tie2, Cdh5, and ephrinB2), and vein (Cd31, Tie2, Cdh5, and EphB4). To detect differentially expressed genes (DEGS), the FindAllMarkers function from Seurat was used. GeneCodis generated top 10 gene-annotation cluster networks of the most significant Panther pathways of all up and down DEGs' P-value < 0.05 (59). An enhanced volcano plot was generated based on the up and down DGEs. GEO accession is #GSE240430.

Adoptive Transfer. The generation of bone marrow chimeric mice was generated as previously described (18). Briefly, adult *EphA4*$^{f/f}$ (WT) or *EphA4*$^{f/f}$*/Tie2-Cre* (KO) male mice at 8 wk of age were exposed to x-ray irradiation (Radsource, Inc.) at 900rads twice, spaced 6 h apart. The next day, irradiated recipient mice received age-matched bone marrow cells from *EphA4*$^{+/+}$*/Tie2-Cre/Rosa26*^{mTmG} (WT BMCs) or *EphA4*$^{f/f}$*/Tie2-Cre/Rosa26*^{mTmG} (KO BMCs) mice. Donor mice express Tie2-Cre from birth with permanent deletion of EphA4 and EGFP expression (60) in endothelial and hematopoietic cells, as we previously described (18, 22).

Cerebral Blood Flow. Cerebral blood flow (CBF) was assessed as previously described (11, 61). Briefly, CBF was assessed at pre-, 5 min, and 1 to 4 dpi using the Moor LDI2-HIR Laser Doppler and Moor Software Version 5.3 (Moor Instruments) using a scanned area of 2.5 cm × 2.5 cm. PFUs were collected using every animal's standard region of interest (ROI). The data were represented as a ratio of postperfusion units (PFU) relative to each animal's preinjury scan.

Statistical Analysis. Data are presented as the SEM and graphed using GraphPad Prism, version 10 (GraphPad Software, Inc.). Comparison between two groups was performed using Student's two-tailed t test. Multiple comparisons between three or more groups using one-way with the post hoc test for multiple comparisons and analysis across time points were performed using repeated measures, two-way ANOVA with post hoc analysis. We constructed a linear mixed effects model to test for mean differences in Ang2 expression over time compared to control samples. The model included time as a fixed effect, a random intercept for subject, and Bonferroni post hoc tests for multiple comparisons. Differences were considered significant if $P < 0.05$.

Data, Materials, and Software Availability. Sequencing data have been deposited in GEO (GSE240430) (62).

ACKNOWLEDGMENTS. We recognize the Biomedical and Veterinary Sciences Program (BMVS) and Megan Frair Naff for sequencing support. We thank John Chappell for the generous gift of the *VE-Cadherin-CreERT2* mice, Dr. Jennifer Munson and Chase Cornelison for shear stress assay support, Monica Ahrens for statistical support, Jordan Daren for clinical coordinating, and Dr. Thomas Cecere for pathology consultation with Christie Lacy for TEM analysis. Funding: This work was supported by the NIH, NS096281(M.H.T. and H.X.), NS112541 (M.H.T. and J.B.M.), and NS121103 (M.H.T.).

1. L. Wilson *et al.*, The chronic and evolving neurological consequences of traumatic brain injury. *Lancet Neurol.* **16**, 813–825 (2017).
2. L. W. Price, G. C. Grant "Frontiers in neuroscience" in *Translational Research in Traumatic Brain Injury*, D. Laskowitz, G. Grant, Eds. (CRC Press/Taylor and Francis Group © 2016 by Taylor & Francis Group, LLC, Boca Raton (FL), 2016).
3. N. J. Abbott, A. A. Patabendige, D. E. Dolman, S. R. Yusof, D. J. Begley, Structure and function of the blood-brain barrier. *Neurobiol. Dis.* **37**, 13–25 (2010).
4. S. M. Stamatovic, R. F. Keep, A. V. Andjelkovic, Brain endothelial cell-cell junctions: How to "open" the blood brain barrier. *Curr. Neuropharmacol.* **6**, 179–192 (2008).
5. R. Cabezas *et al.*, Astrocytic modulation of blood brain barrier: Perspectives on Parkinson's disease. *Front. Cell Neurosci.* **8**, 211 (2014).
6. J. I. Alvarez, T. Katayama, A. Prat, Glial influence on the blood brain barrier. *Glia* **61**, 1939–1958 (2013).
7. C. Suri *et al.*, Requisite role of angiopoietin-1, a ligand for the TIE2 receptor, during embryonic angiogenesis. *Cell* **87**, 1171–1180 (1996).
8. S. Michinaga, Y. Koyama, Dual roles of astrocyte-derived factors in regulation of blood-brain barrier function after brain damage. *Int. J. Mol. Sci.* **20**, 571 (2019).
9. L. Jiang *et al.*, Selective suppression of the JNK-MMP2/9 signal pathway by tetramethylpyrazine attenuates neuropathic pain in rats. *J. Neuroinflamm.* **14**, 174 (2017).
10. H. Min *et al.*, TLR2-induced astrocyte MMP9 activation compromises the blood brain barrier and exacerbates intracerebral hemorrhage in animal models. *Mol. Brain* **8**, 23 (2015).
11. B. Okyere *et al.*, EphA4/Tie2 crosstalk regulates leptomeningeal collateral remodeling following ischemic stroke. *J. Clin. Invest.* **130**, 1024–1035 (2020).
12. N. J. Xu, M. Henkemeyer, Ephrin reverse signaling in axon guidance and synaptogenesis. *Semin. Cell Dev. Biol.* **23**, 58–64 (2012).
13. E. B. Pasquale, Eph-ephrin bidirectional signaling in physiology and disease. *Cell* **133**, 38–52 (2008).
14. E. M. Lisabeth, G. Falivelli, E. B. Pasquale, Eph receptor signaling and ephrins. *Cold Spring Harb Perspect. Biol.* **5**, a009159 (2013).
15. Y. Zhang *et al.*, An RNA-sequencing transcriptome and splicing database of glia, neurons, and vascular cells of the cerebral cortex. *J. Neurosci.* **34**, 11929–11947 (2014).
16. S. Teng *et al.*, Inhibition of EphA/Ephrin-A signaling using genetic and pharmacologic approaches improves recovery following traumatic brain injury in mice. *Brain Inj.* **33**, 1385–1401 (2019).
17. J. Bai, Y. J. Wang, L. Liu, Y. L. Zhao, Ephrin B2 and EphB4 selectively mark arterial and venous vessels in cerebral arteriovenous malformation. *J. Int. Med. Res.* **42**, 405–415 (2014).
18. E. A. Kowalski *et al.*, Peripheral loss of EphA4 ameliorates TBI-induced neuroinflammation and tissue damage. *J. Neuroinflamm.* **16**, 210 (2019).
19. J. Thundyil *et al.*, Evidence that the EphA2 receptor exacerbates ischemic brain injury. *PLoS One* **8**, e53528 (2013).
20. M. A. Venneri *et al.*, Identification of proangiogenic TIE2-expressing monocytes (TEMs) in human peripheral blood and cancer. *Blood* **109**, 5276–5285 (2007).
21. Y. Tang, A. Harrington, X. Yang, R. E. Friesel, L. Liaw, The contribution of the Tie2+ lineage to primitive and definitive hematopoietic cells. *Genesis* **48**, 563–567 (2010).
22. B. Okyere *et al.*, Endothelial-specific EphA4 negatively regulates native pial collateral formation and re-perfusion following hindlimb ischemia. *PLoS One* **11**, e0159930 (2016).
23. M. A. Erickson, T. Shulyatnikova, W. A. Banks, M. R. Hayden, Ultrastructural remodeling of the blood-brain barrier and neurovascular unit by lipopolysaccharide-induced neuroinflammation. *Int. J. Mol. Sci.* **24**, 1640 (2023).
24. A. S. Lossinsky, R. R. Shivers, Structural pathways for macromolecular and cellular transport across the blood-brain barrier during inflammatory conditions. Review. *Histol. Histopathol.* **19**, 535–564 (2004).
25. J. H. Seo *et al.*, AKAP12 supports blood-brain barrier integrity against ischemic stroke. *Int. J. Mol. Sci.* **21**, 9078 (2020).
26. S. Akakura, I. H. Gelman, Pivotal role of akap12 in the regulation of cellular adhesion dynamics: Control of cytoskeletal architecture, cell migration, and mitogenic signaling. *J. Signal Transduct.* **2012**, 529179 (2012).
27. Y. K. Choi *et al.*, AKAP12 regulates human blood-retinal barrier formation by downregulation of hypoxia-inducible factor-1alpha. *J. Neurosci.* **27**, 4472–4481 (2007).
28. H. Li, Physiologic and pathophysiologic roles of AKAP12. *Sci. Prog.* **105**, 368504221109212 (2022).
29. P. Kumpers *et al.*, The synthetic tie2 agonist peptide vasculotide protects against vascular leakage and reduces mortality in murine abdominal sepsis. *Crit. Care* **15**, R261 (2011).
30. S. Gurnik *et al.*, Angiopoietin-2-induced blood-brain barrier compromise and increased stroke size are rescued by VE-PTP-dependent restoration of Tie2 signaling. *Acta Neuropathol.* **131**, 753–773 (2016).
31. A. L. C. Schneider *et al.*, Associations of microvascular injury-related biomarkers with traumatic brain injury severity and outcomes: A transforming research and clinical knowledge in traumatic brain injury (TRACK-TBI) pilot study. *J. Neurotrauma.* **40**, 1625–1637 (2023), 10.1089/neu.2022.0442.
32. E. Soliman *et al.*, Conditional deletion of EphA4 on Cx3cr1-expressing microglia fails to influence histopathological outcome and blood brain barrier disruption following brain injury. *Front. Mol. Neurosci.* **14**, 747770 (2021).
33. A. C. Luissint, C. Artus, F. Glacial, K. Ganeshamoorthy, P. O. Couraud, Tight junctions at the blood brain barrier: Physiological architecture and disease-associated dysregulation. *Fluids Barriers CNS* **9**, 23 (2012).
34. A. Ghori *et al.*, EphrinB2 activation enhances vascular repair mechanisms and reduces brain swelling after mild cerebral ischemia. *Arterioscler. Thromb Vasc Biol.* **37**, 867–878 (2017).
35. T. K. Darling *et al.*, EphA2 contributes to disruption of the blood-brain barrier in cerebral malaria. *PLoS Pathog.* **16**, e1008261 (2020).
36. T. A. Bowden *et al.*, Structural plasticity of Eph-receptor A4 facilitates cross-class ephrin signaling. *Structure* **17**, 1679 (2009).
37. K. Kajiya *et al.*, Promotion of lymphatic integrity by angiopoietin-1/Tie2 signaling during inflammation. *Am. J. Pathol.* **180**, 1273–1282 (2012).
38. K. E. Milam, S. M. Parikh, The angiopoietin-Tie2 signaling axis in the vascular leakage of systemic inflammation. *Tissue Barriers* **3**, e957508 (2015).
39. L. Claesson-Welsh, E. Dejana, D. M. McDonald, Permeability of the endothelial barrier: Identifying and reconciling controversies. *Trends Mol. Med.* **27**, 314–331 (2021).
40. P. Saharinen, L. Eklund, K. Alitalo, Therapeutic targeting of the angiopoietin-TIE pathway. *Nat. Rev. Drug Discov.* **16**, 635–661 (2017).
41. M. Trieu *et al.*, Vasculotide, an angiopoietin-1 mimetic, restores microcirculatory perfusion and microvascular leakage and decreases fluid resuscitation requirements in hemorrhagic shock. *Anesthesiology* **128**, 361–374 (2018).
42. B. Gutbier *et al.*, Vasculotide reduces pulmonary hyperpermeability in experimental pneumococcal pneumonia. *Crit. Care* **21**, 274 (2017).
43. E. Rubig *et al.*, The synthetic Tie2 agonist peptide vasculotide protects renal vascular barrier function in experimental acute kidney injury. *Sci. Rep.* **6**, 22111 (2016).
44. U. Fiedler *et al.*, The Tie-2 ligand angiopoietin-2 is stored in and rapidly released upon stimulation from endothelial cell Weibel-Palade bodies. *Blood* **103**, 4150–4156 (2004).
45. J. H. Cha *et al.*, AKAP12 mediates barrier functions of fibrotic scars during CNS repair. *PLoS One* **9**, e94695 (2014).
46. H. B. Kwon *et al.*, AKAP12 regulates vascular integrity in zebrafish. *Exp. Mol. Med.* **44**, 225–235 (2012).
47. H. Qasim, B. K. McConnell, AKAP12 signaling complex: Impacts of compartmentalizing cAMP-dependent signaling pathways in the heart and various signaling systems. *J. Am. Heart Assoc.* **9**, e016615 (2020).

48. Y. Zhang, C. D. Kontos, B. H. Annex, A. S. Popel, A systems biology model of junctional localization and downstream signaling of the Ang-Tie signaling pathway. *NPJ Syst. Biol. Appl.* **7**, 34 (2021).
49. L. F. Ribeiro, J. de Wit, Neuronal polarity: MAP2 shifts secretory vesicles into high gear for long-haul transport down the axon. *Neuron* **94**, 223–225 (2017).
50. Y. Cao *et al.*, Microtubule minus-end binding protein CAMSAP2 and Kinesin-14 motor KIFC3 control dendritic microtubule organization. *Curr. Biol.* **30**, 899–908.e896 (2020).
51. A. H. Rasmussen, H. B. Rasmussen, A. Silahtaroglu, The DLGAP family: Neuronal expression, function and role in brain disorders. *Mol. Brain* **10**, 43 (2017).
52. L. A. Elferink, K. Anzai, R. H. Scheller, rab15, a novel low molecular weight GTP-binding protein specifically expressed in rat brain. *J. Biol. Chem.* **267**, 5768–5775 (1992).
53. T. R. Brickler *et al.*, Angiopoietin/Tie2 axis regulates the age-at-injury cerebrovascular response to traumatic brain injury. *J. Neurosci.* **38**, 9618–9634 (2018).
54. P. Van Slyke *et al.*, Acceleration of diabetic wound healing by an angiopoietin peptide mimetic. *Tissue Eng. Part A* **15**, 1269–1280 (2009).
55. M. I. Love, W. Huber, S. Anders, Moderated estimation of fold change and dispersion for RNA-seq data with DESeq2. *Genome Biol.* **15**, 550 (2014).
56. W. Huang da, B. T. Sherman, R. A. Lempicki, Systematic and integrative analysis of large gene lists using DAVID bioinformatics sources. *Nat. Protoc.* **4**, 44–57 (2009).
57. W. Huang da, B. T. Sherman, R. A. Lempicki, Bioinformatics enrichment tools: Paths toward the comprehensive functional analysis of large gene lists. *Nucleic Acids Res.* **37**, 1–13 (2009).
58. A. Butler, P. Hoffman, P. Smibert, E. Papalexi, R. Satija, Integrating single-cell transcriptomic data across different conditions, technologies, and species. *Nat. Biotechnol.* **36**, 411–420 (2018).
59. A. Garcia-Moreno *et al.*, Functional enrichment analysis of regulatory elements. *Biomedicines* **10**, 590 (2022).
60. M. D. Muzumdar, B. Tasic, K. Miyamichi, L. Li, L. Luo, A global double-fluorescent Cre reporter mouse. *Genesis* **45**, 593–605 (2007).
61. B. Okyere, M. Creasey, Y. Lebovitz, M. H. Theus, Temporal remodeling of pial collaterals and functional deficits in a murine model of ischemic stroke. *J. Neurosci. Methods* **293**, 86–96 (2018).
62. A. Cash, H. Xie, M. Theus, Endothelial deletion of EPH receptor A4 alters single-cell profile and Tie2/Akap12 signaling to preserve blood-brain barrier integrity. NCBI, Gene Expression Omnibus. https://www.ncbi.nlm.nih.gov/geo/query/acc.cgi?acc=GSE240430. Accessed 24 September 2023.